



Discovery of novel indole derivatives that inhibit NEDDylation and MAPK pathways against gastric cancer MGC803 cells

Dong-Jun Fu^a, Xin-Xin Cui^b, Ting Zhu^b, Yan-Bing Zhang^b, Yang-Yang Hu^e, Li-Rong Zhang^{b,c,d}, Sheng-Hui Wang^{b,c,d}, Sai-Yang Zhang^{b,c,d,f,*}

^a Modern Research Center for Traditional Chinese Medicine, School of Chinese Materia Medica, Beijing University of Chinese Medicine, Beijing 100029, China

^b School of Basic Medical Science, Zhengzhou University, Zhengzhou 450001, China

^c The Academy of Medical Science, Zhengzhou University, Zhengzhou 450001, China

^d Henan Institute of Advanced Technology, Zhengzhou University, Zhengzhou 450001, China

^e Faculty of Science, The University of Melbourne, Victoria 3010, Australia

^f State Key Laboratory of Pharmaceutical Biotechnology, Nanjing University, Nanjing 210023, Jiangsu, China

ARTICLE INFO

Keywords:

Indole
Apoptosis
NEDDylation pathway
MAPK pathway
MGC803 cells

ABSTRACT

A series of novel indole derivatives were synthesized and evaluated for their antiproliferative activity against three selected cancer cell lines (MGC803, EC-109 and PC-3). Among these analogues, 2-(5-methoxy-1*H*-indol-1-yl)-*N*-(4-methoxybenzyl)-*N*-(3,4,5-trimethoxyphenyl)acetamide (**V7**) showed the best inhibitory activity against MGC803 cells with an IC₅₀ value of 1.59 μM. Cellular mechanisms elucidated that **V7** inhibited colony formation, induced apoptosis and arrested cell cycle at G2/M phase. Importantly, indole analogue **V7** inhibited NEDDylation pathway and MAPK pathway against MGC803 cells.

1. Introduction

Neddylation, a 3-step enzymatic cascade involving NEDD8-activating enzyme (NAE3/UBA3, E1), NEDD8-conjugating enzyme E2 (UBC12 or UBE2F) and substrate-specific E3s, regulates a variety of biological processes by affecting the subcellular localization, stability, conformation and function of target proteins [1–3]. Recently, accumulated experimental data reported that the levels of Neddylation enzymes (e.g. NEDD8 E1 and NAE1/UBA3) are higher in human cancers, including gastric cancer, lung cancer, liver cancer, esophagus cancer and colorectal cancer, when compared to adjacent normal tissues [4,5]. Thus, elevated status of Neddylation modification might be an oncogenic event during carcinogenesis, leading to degradation and ubiquitylation of many tumor suppressor substrates (e.g. ATF4, c-myc and p21) [6]. Scheme 1.

Inhibition of protein Neddylation has emerged as a promising anticancer strategy since the discovery of the NAE inhibitor MLN4924 (Fig. 1), and MLN4924 is currently in several phase I and II clinical trials for cancer therapy [7–10]. However, as a result of its broad ablation of Neddylation, MLN4924 has a series of toxicities [11]. Compound 2 could inhibit the DCN1-UBE2M protein–protein interaction in the TR-

FRET binding assay and inhibit cullin NEDDylation in the pulse-chase NEDD8 transfer assay [12]. In addition, some NAE inhibitors has been reported, such as compounds 3–6, but while there still were some shortages about potency and druglike physical properties in those compounds [13]. Nucleoside analogue 7 as an NAE and UAE dual inhibitor inhibited conjugation of ubiquitin to intracellular proteins and prevented the formation of cytoprotective aggresomes in A549 lung cancer cells [14].

In continuation with our efforts toward the identification of Neddylation inhibitors with anticancer potential, we attempt to discovery structurally diverse scaffolds to design novel Neddylation inhibitors. Recently, our group has reported three Neddylation inhibitors (Fig. 2): (1) **DC-2** specifically inhibited the interactions of DCN1 and UBE2M at molecule and cellular levels, resulting in the decrease of cullin3 Neddylation and accumulation of its substrate [15]; (2) **WS-383** inhibited Cul3/1 Neddylation selectively over other cullins and also induced accumulation of p21, p27, and NRF2 against MGC803 cells [16]; (3) **Flavokawain B** inhibited NEDD8 conjugations to both Cullin1 and Ubc12 in prostate cancer cell lines [17].

Indoles as one of the most abundant heterocycles among biologically active natural products and chemical agents possess interesting

* Corresponding author at: School of Basic Medical Science, Zhengzhou University, Zhengzhou 450001, China.

E-mail addresses: zzufdj@sina.com (D.-J. Fu), saiyangz@zzu.edu.cn (S.-Y. Zhang).

<https://doi.org/10.1016/j.bioorg.2021.104634>

Received 8 September 2020; Received in revised form 3 January 2021; Accepted 4 January 2021

Available online 8 January 2021

0045-2068/© 2021 Elsevier Inc. All rights reserved.

pharmacological properties [18–20]. Importantly, various indoles were designed and synthesized as potential anticancer candidates [21,22]. To discover more potent Neddylation inhibitors and anticancer agents [23–32], we synthesized a series of novel indole derivatives based on the anticancer indole scaffold. In this work, synthetic indoles were evaluated for their antiproliferative activity against three cancer cell lines (EC-109, PC-3 and MGC803). Among them, indole **V7** was evaluated for its apoptosis and deneddylation effects in gastric cancer MGC803 cells. Our findings in this work might suggest that the indole would be a new scaffold for the development of NEDDylation inhibitors.

2. Results and discussion

2.1. Chemistry

The synthetic route of novel indole derivatives was shown in Scheme 1. Phenylamine derivatives **I** was subjected to nucleophilic substitution reaction with benzyl chloride analogues **II** to afford secondary amine **III** in the presence of potassium carbonate. The intermediate **III** was reacted with chloroacetyl chloride to obtain the tertiary amide analogues **IV** in the ethyl acetate solvent system. The target analogues **V1 ~ V17** were easily obtained at the reflux condition with 5-methoxy-1H-indole in the presence of sodium hydroxide. The structure confirmation and NMR analysis of indole derivatives **V1 ~ V17** were described in the Supporting Information.

2.2. Antiproliferative activity evaluation

In order to discover potent anticancer agents and potential Neddylation pathway inhibitors, we evaluated the anticancer activity *in vitro* of all indole derivatives **V1 ~ V17** against cancer cell lines (PC-3, MGC803 and EC-109) using the MTT assay. In this paper, 5-fluorouracil (**5-Fu**) was used as the control drug in the MTT assay. The anticancer activity *in vitro* results against all three cancer cells for indole derivatives **V1 ~ V17** were shown in Table 1.

To explore the effect of substituent groups on the phenyl ring A for inhibitory activity, different electron-withdrawing groups and electron-donating groups were introduced into the targeted compounds. All these indole derivatives **V1 ~ V14** exhibited the effective activity against MGC803 cells and EC-109 cells. Especially, 2-(5-methoxy-1H-indol-1-yl)-N-(4-methoxybenzyl)-N-(3,4,5-trimethoxyphenyl)acetamide (**V7**) showed the most excellent antiproliferative activity with an IC₅₀ value of

1.59 μM against MGC803 cancer cells. The relationships between the halogen substituents and the antiproliferative activities were 4-Br > 4-Cl > 4-F. Compounds **V6 ~ V10**, **V12** and **V14** with electron-donating groups on the phenyl ring A displayed moderate to potent inhibitory effects against all cancer cells with IC₅₀ values from 1.59 μM to 71.83 μM. Replacing the 4-OCH₃ of **V7** with 4-CH₃ of **V6** led to a decrease of the anticancer activity *in vitro* against all cancer cells. However, changing the 4-C(CH₃)₃ of **V9** to 3-OCH₃ of **V12** led to a significant improvement of the activity against MGC803, PC-3 and EC-109 cell lines. These inhibitory results indicate that substituent groups on the phenyl ring A exhibited an important effect for the anticancer activity *in vitro*.

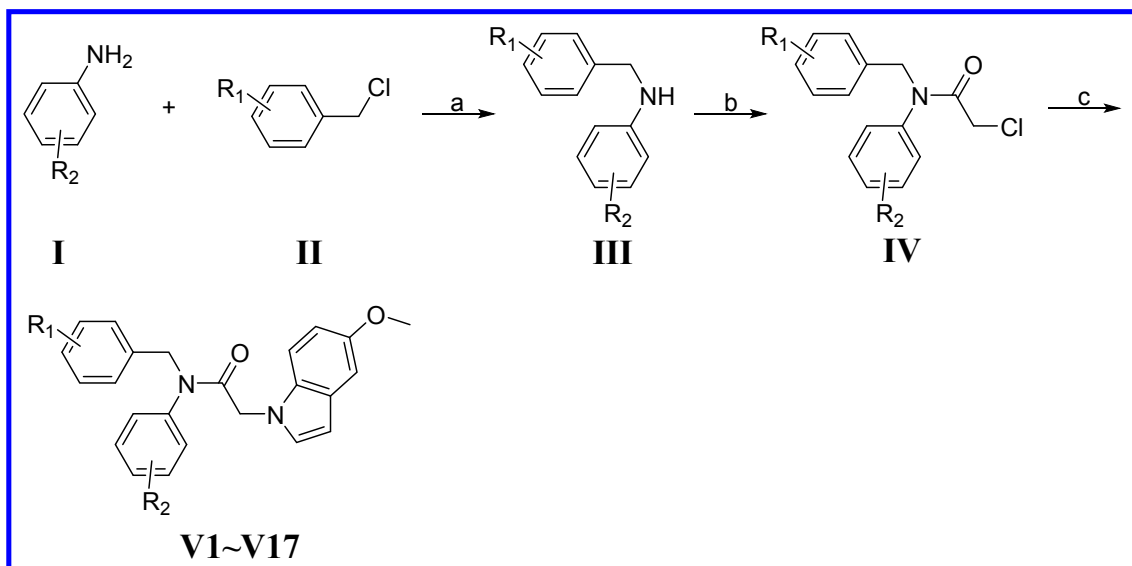
In addition, the importance of 3,4,5-triOCH₃ group on the phenyl ring B for inhibitory activity was also explored. When the 3,4,5-triOCH₃ group was replaced by 3,4-diOCH₃, 4-OCH₃, or hydrogen atom, the antiproliferative activity was obviously decreased. Indole derivatives **V15 ~ V17** exhibited very weak activity with IC₅₀ values of > 80 μM against PC-3 and EC-109 cell lines.

2.3. Compound V7 selectively inhibited the viability against gastric cancer cells

Based on the results of inhibitory activities, compound **V7** was selected to explore its cell viabilities against gastric cancer MGC803 cells, HGC-27 cells, SGC-7901 cells, and normal GES-1 cells. Among all four cell lines, compound **V7** displayed best antiproliferative activity against MGC803 cells in a concentration dependent manner (Fig. 3A). The viability of MGC803 cells after the 2 μmol/L treatment is approximately 28%, while the viability of GES-1 cells remains higher than 78%. In addition, compound **V7** inhibited the growth against MGC803 cells, HGC-27 cells and SGC-7901 cells in a time-dependent manner (Fig. 3B). Taking the results together, **V7** selectively inhibited the viability against gastric cancer cells.

2.4. Compound V7 caused proliferation inhibition against MGC803 cells

In order to evaluate the proliferation ability of indole **V7** against MGC803 cells, the effects of cell morphology changes and colony formation were also evaluated. MGC803 cell morphology changes after 48 h treatment were shown in Fig. 4A. As the concentration increased, cells rounding up and cell debris were observed especially at high concentrations. We next checked the growth rate influenced by **V7**. As shown in



Scheme 1. Reagents and conditions: (a) K₂CO₃, acetone, reflux; (b) chloroacetyl chloride, ethyl acetate, rt; (c) NaOH, 5-methoxy-1H-indole, acetone, reflux.

the Fig. 4B and Fig. 4D, MGC803 cells were co-incubated with different concentrations of **V7** to determine the effects on forming colonies. After 7 days incubation, the cell colonies were obviously decreased by compound **V7**. We next checked the growth effects influenced by **V7**. As shown in the Fig. 4C, following the treatment with compound **V7**, the viability of MGC803 cells was decreased in concentration-dependent and time-dependent manners. All these results revealed that **V7** inhibited the cell proliferation.

2.5. 2.5 compound **V7** induced the apoptosis against MGC803 cells

In order to explore the apoptotic effects, 4',6-diamidino-2-phenylindole (DAPI) staining was performed in MGC803 cells. Some remarkable nuclear changes including nuclear fragmentation and condensation were observed when MGC803 cells were treated with **V7** (Fig. 5A).

MGC803 cells were analyzed after stained by Annexin V-FITC/PI to determine the apoptosis percentages. As shown in Fig. 5B, apoptosis effects of MGC803 cells was induced by compound **V7**. From the right panel, it revealed the apoptosis percentages in MGC803 cells after treated by **V7**. Treatment of MGC803 cells with compound **V7** resulted in a concentration-dependent increase (Fig. 5C), and the percentage of apoptotic cells was up to 4.4%, 11.1%, and 65.2%, respectively, compared to the control (3.2%).

MGC803 cells were analyzed after stained by Annexin V-FITC/PI to determine the apoptosis percentages. As shown in Fig. 5B, apoptosis effects of MGC803 cells was induced by compound **V7**. From the right panel, it revealed the apoptosis percentages in MGC803 cells after treated by **V7**. Treatment of MGC803 cells with compound **V7** resulted in a concentration-dependent increase (Fig. 5C), and the percentage of apoptotic cells was up to 4.4%, 11.1%, and 65.2%, respectively, compared to the control (3.2%).

2.6. Compound **V7** activated extrinsic and intrinsic apoptosis pathways against MGC803 cells

Apoptosis is a very tightly programmed cell death with distinct biochemical and genetic pathways that play a critical role in the homeostasis of cancer cells [33]. The process of apoptosis is triggered by

two different signaling pathways. The extrinsic apoptotic signal, which responded mainly to extracellular stimuli, involves death receptors, and the intrinsic apoptotic process, activated by modulators within the cell itself, involves the mitochondria [34]. The complex interplay between proapoptotic and antiapoptotic members of the Bcl-2 family plays a crucial role in cellular fate determination [35].

As shown in Fig. 6, Bcl-2 family members highly involved in intrinsic mitochondria apoptosis pathway were detected. The pro-apoptosis protein Bax was upregulated, while the anti-apoptosis protein Bcl-2 and Bcl-xL were downregulated. The executors Caspase 3/7 were evidently activated, and their substrate PARP was also activated by **V7** in a concentration dependent manner. The important apoptosis inhibitor cIAP1 was down-regulated. All these results suggested that **V7** induced cell apoptosis of MGC803 cells in an extrinsic and intrinsic combined pathway.

2.7. Compound **V7** arrested cell cycle at G2/M phase and induced DNA damage

Cell cycle checkpoint mechanisms are crucial for the protection and maintenance of genome integrity during tumorigenesis [36]. Cell cycle progression is tightly controlled by cyclins and cyclin-dependent kinases (CDKs), the sequential activation of which allows for the initiation of and transition between different phases of the cell cycle [37]. Results in Fig. 7A&B showed that **V7** arrested cell cycle at G2/M phase concentration-dependently. In addition, **V7** decreased the expression level of p-Histone H3 in MGC803 cells (Fig. 7C). The expression levels of CDK1 and CyclinB1 in MGC803 cells were unchanged.

DNA repair can determine fate of a cell with treatment stress which either resists over to survive or respond to toxic agents [38]. When the repair mechanisms are unsuccessful, it may cause cellular senescence (permanent cell cycle arrest), oncogenesis, normal embryonic development, and maintenance of cell homeostasis [39]. In the comet assay, the tail lengths of comet were lengthened by **V7** (Fig. 7D). These results indicated that **V7** caused a strong DNA damage in MGC803 cells.

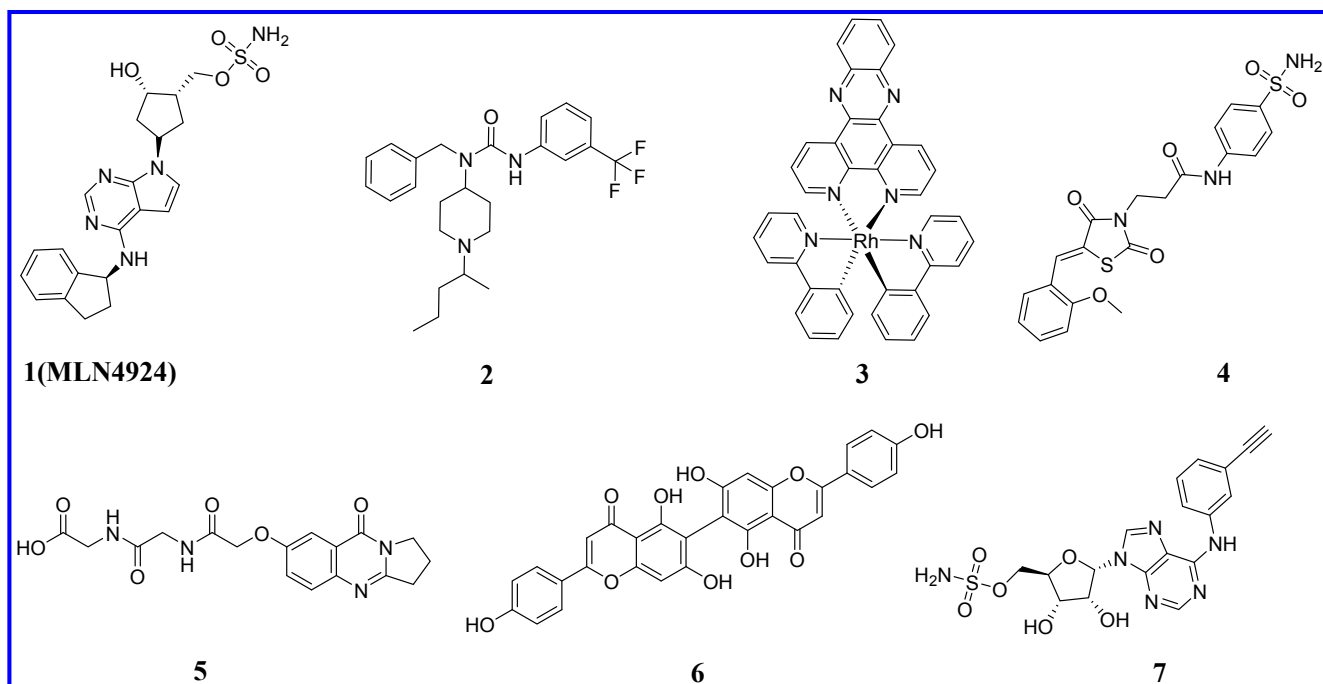


Fig. 1. Structures of reported NEDDylation inhibitors in other groups.

2.8. Compound V7 inhibited the MAPK pathway

Mitogen-activated protein kinase (MAPK) pathway is a critical pathway for human cancer cell survival [40]. There are three independent MAPK pathways composed of three signaling families closely related to cell proliferation: the ERK family, the P38 family and the JNK family [41]. It has been originally shown that ERKs are important for cell survival, whereas JNKs and p38-MAPKs were deemed stress responsive and thus involved in apoptosis [42,43].

Biomarker of each pathway was chosen to determine the effect of V7 on MAPK. As shown in the Fig. 8, p-c-Jun was not regulated by V7, while p-ERK and p-P38 have been down-regulated. Among them, p-ERK has a most significant change, so we detected the up-stream proteins nextly. Results showed that c-Raf, p-c-Raf, p-MEK1/2 and p-ERK1/2 were down-regulated while Ras remained the same. All these results indicated that compound V7 inhibited the MAPK pathway in MGC803 cells.

Co-incubating with V7, proteasome inhibitor MG132 did not recover the down-regulation of c-Raf and p-c-Raf (Fig. 9A). Moreover, compound V7 cannot promote the degradation of c-Raf and p-c-Raf (Fig. 9B). Results here suggested the down-regulation of p-c-Raf by V7 is not the result of promoting the degradation of p-c-Raf. V7 inhibited the activity of Ras to have an influence on the phosphorylation of c-Raf.

Taking these together, V7 may inhibit the expression of c-Raf, then inhibit the activation of MEK1/2 and ERK1/2 resulting in the cell proliferation inhibition.

2.9. Compound V7 inhibited NEDDylation

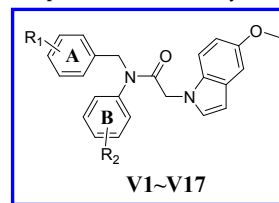
To discovery a novel NEDDylation inhibitor, the effects of V7 on NEDDylation were detected. In an *in vitro* NEDD8 conjugation assay, V7 inhibited the conjugation of Ubc12 and NEDD8 formatting Ubc12-NEDD8, the band of Ubc12-NEDD8 is getting smaller evidently with the effect of 2803 (Fig. 10A).

Inner the MGC803 cells, V7 also inhibited the NEDDylation of NEDDylation E1 (NAE1) and two members of NEDDylation E3 complexes (Cullin 1 and Cullin 3). In Fig. 10B, the NEDDylation of each protein (with one NEDD8 conjugated, the NEDDylation band will be 9 kDa higher than the original proteins) were significantly inhibited by V7. To see the overall effect of V7 on NEDDylation, the whole protein lysate was used to do the western blotting with anti-NEDD8. As shown in the Fig. 10C, V7 inhibited the general tendency of NEDDylation inner MGC803 cells. Nextly, we checked the two important NEDDylation substrates involved in cell death and proliferation. Both Death Receptor 5 (DR5) and P21 were clearly accumulated as a result of NEDDylation inhibition (Fig. 10E). To sum up, V7 inhibited NEDDylation in a concentration dependent manner against MGC803 cells.

The biological tests have proved that compound V7 interacted with NAE1 regulatory subunit to inhibit UBC12 NEDDylation in MGC-803 cells. Based on this, a docking study was performed to explore the detailed interactions between compound V7 and NAE (PDB code: 3GZN,

Table 1

Antiproliferative activity of the indole derivatives V1 ~ V17.



Compound	R ₁	R ₂	IC ₅₀ (μM) ^a		
V1	H	3,4,5-triOCH ₃	EC-109 47.57 ± 2.52	PC-3 >80	MGC803 22.59 ± 1.74
V2	4-F	3,4,5-triOCH ₃	47.77 ± 3.50	>80	43.47 ± 1.11
V3	4-Cl	3,4,5-triOCH ₃	46.82 ± 2.89	34.53 ± 1.52	51.52 ± 1.12
V4	4-Br	3,4,5-triOCH ₃	29.07 ± 0.84	21.23 ± 1.48	25.09 ± 1.64
V5	3-F	3,4,5-triOCH ₃	64.61 ± 3.08	>80	20.69 ± 1.87
V6	4-CH ₃	3,4,5-triOCH ₃	21.00 ± 0.44	18.04 ± 0.84	7.62 ± 0.04
V7	4-OCH ₃	3,4,5-triOCH ₃	14.52 ± 0.29	3.56 ± 0.08	1.59 ± 0.01
V8	3-CH ₃	3,4,5-triOCH ₃	39.40 ± 0.64	43.83 ± 2.55	64.67 ± 2.59
V9	4-C (CH ₃) ₃	3,4,5-triOCH ₃	58.25 ± 1.16	8.36 ± 0.22	34.55 ± 0.77
V10	2-CH ₃	3,4,5-triOCH ₃	71.83 ± 4.67	39.03 ± 1.11	18.56 ± 0.86
V11	3-Cl	3,4,5-triOCH ₃	37.45 ± 0.83	38.09 ± 0.77	66.93 ± 2.37
V12	3-OCH ₃	3,4,5-triOCH ₃	7.58 ± 0.65	7.01 ± 0.17	19.04 ± 1.95
V13	3-CH ₂ Cl	3,4,5-triOCH ₃	52.08 ± 0.51	18.94 ± 0.47	36.57 ± 0.56
V14	3,5-diOCH ₃	3,4,5-triOCH ₃	37.45 ± 0.83	38.09 ± 0.77	66.93 ± 2.37
V15	4-OCH ₃	H	>80	>80	19.43 ± 0.82
V16	4-OCH ₃	4-OCH ₃	>80	>80	>80
V17	4-OCH ₃	3,4-diOCH ₃	>80	>80	>80
5-Fu	-	-	15.53 ± 0.27	12.87 ± 1.10	8.22 ± 0.56

^a Antiproliferative activity was assayed by exposure for 48 h.

resolution: 3.00 Å). We could find that compound V7 could be well docked in the active cavity of NAE (Fig. 10D). Its 4-methoxyl-phenyl group was located in a hydrophobic pocket consist of Ile75, Met101, Lys147, Ile148, Leu166 and Ala171. Meanwhile, the 4-methoxyl-phenyl group had a hydrogen bond with the backbone of Ile148. The 3,4,5-trimethoxyl-phenyl group could have hydrophobic interaction with Met101, Ala170, Ile309 and Ile310, and form a hydrogen bond with

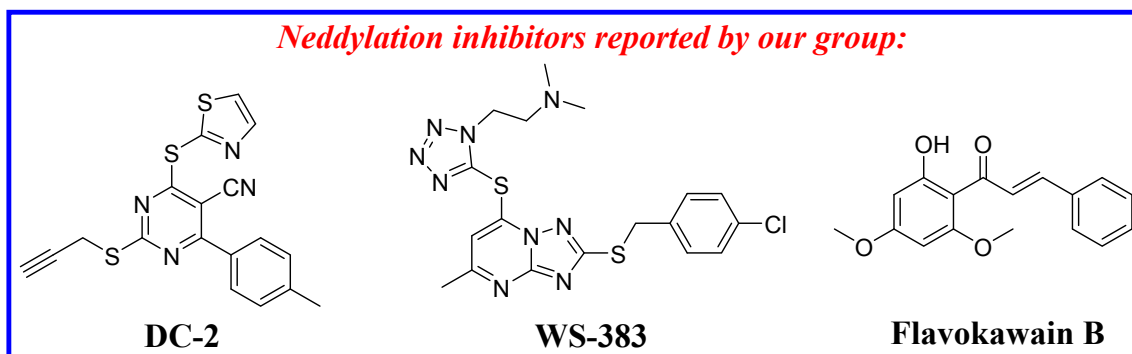


Fig. 2. NEDDylation inhibitors reported by our group.

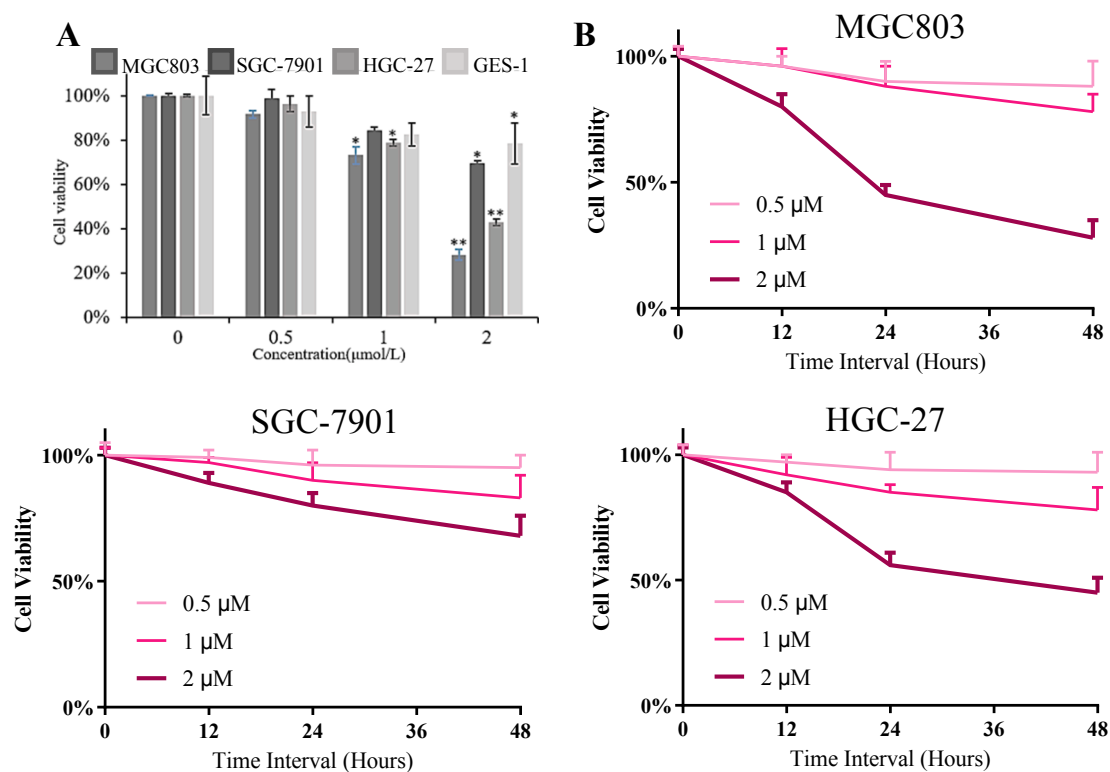


Fig. 3. A. Cell viabilities of different cell lines with the treatment of V7 for 48 h treatment; B. Cell viabilities of MGC803 cells, HGC-27 cells and SGC-7901 cells with the treatment of V7 for different hours. The results shown were representative of three independent experiments. *: $p < 0.05$ verse control. **: $p < 0.01$ verse control.

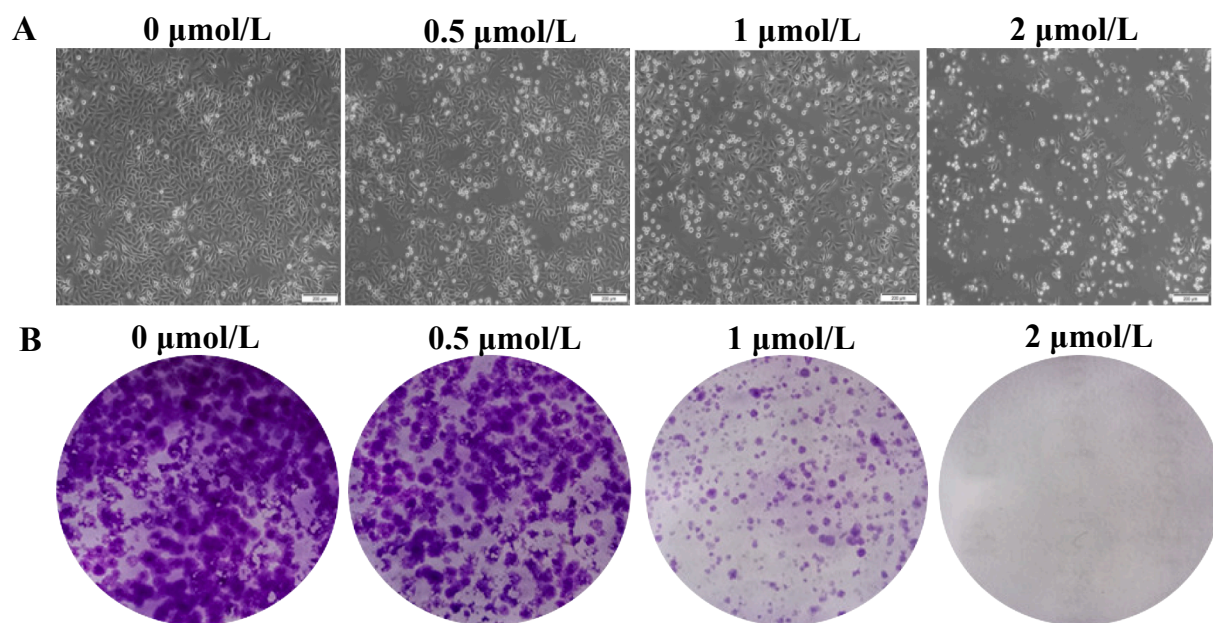


Fig. 4. A. Cell morphology changes of MGC803 cells after 48 h treatment; B. Representative images of MGC803 cells colonies after treatment for a week; C. Growth curve of MGC803 cells; D. Statistical analysis of colony formation rates. The results shown were representative of three independent experiments. **: $p < 0.01$ verse control. ****: $p < 0.0001$ verse control.

Ser168. Moreover, the 5-methoxy-indole group has hydrophobic interaction with surrounding residues Leu80, Lys124, Asp167, Thr203 and Ile310. The 5-methoxy-indole group could also form hydrogen bonds with Leu80 and Lys124. From the docking result, we could find compound V7 could bind to NAE via hydrogen bonds and hydrophobic interactions and therefore inhibit NAE as well as NEDD8 pathway, which could explain the good anticancer activity of compound V7.

3. Conclusion

A series of indole derivatives were synthesized and evaluated for their antiproliferative activity against PC-3, MGC803 and EC-109 cells. Among all these analogues, compound V7 possessed the best antiproliferative ability with an IC_{50} value of 1.59 μM against MGC803 cells. Compound V7 could inhibit MGC803 cell growth selectively and

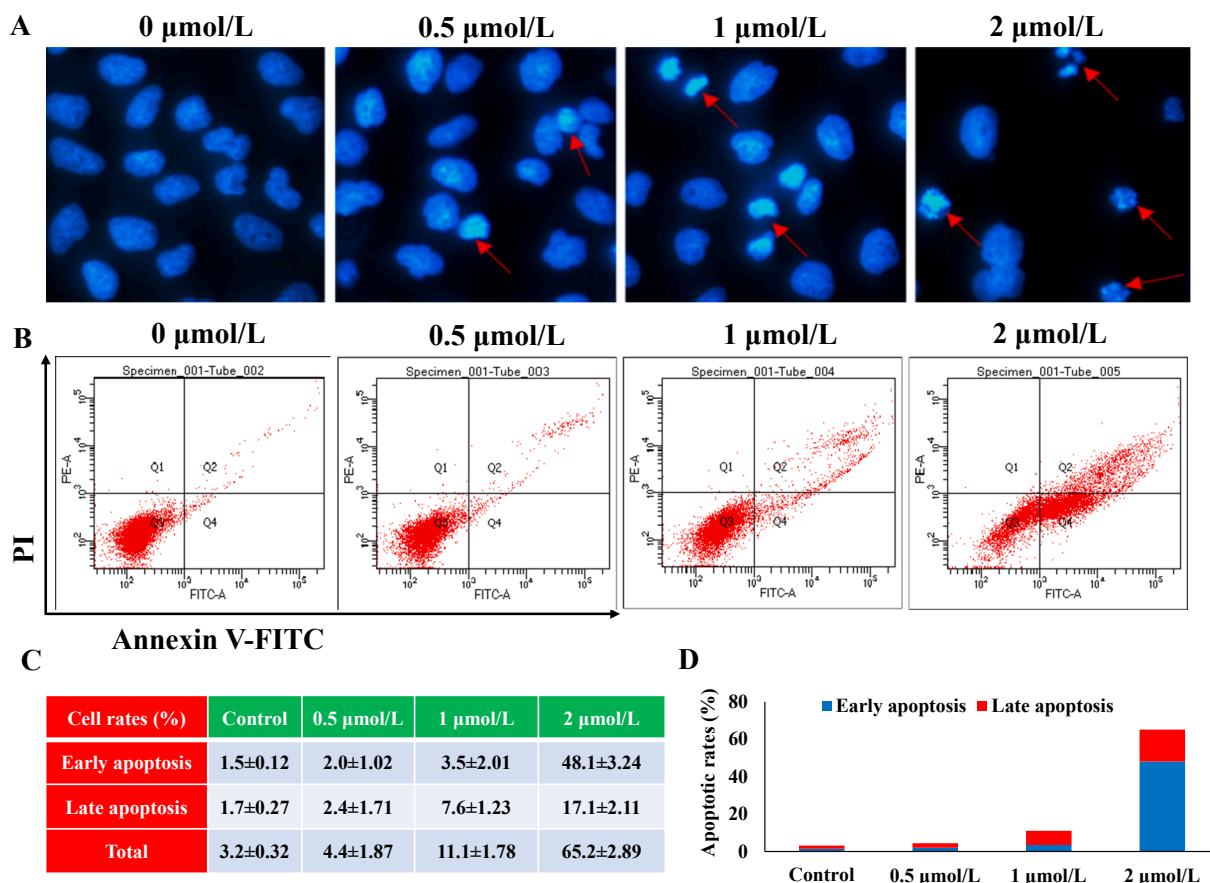


Fig. 5. **A**. MGC803 cells were stained by DAPI after 48 h treatment, red arrows were drawn to point out the nuclear condensation; **B**. MGC803 cells were stained by Annexin V-FITC/PI and analyzed by flow cytometry after 48 h treatment; **C&D**. Apoptotic rates of MGC803 cells. (For interpretation of the references to colour in this figure legend, the reader is referred to the web version of this article.)

arrest cell cycle at G2/M phase. Importantly, indole **V7** inhibited NEDDylation and MAPK pathways against MGC803 cells, which led to activated extrinsic and intrinsic apoptosis pathways (Fig. 11). From the results of docking analysis, compound **V7** could bind to NEDD8 activating enzyme (NAE) via hydrogen bonds and hydrophobic interactions. It suggested that the indole derivative **V7** as a NEDDylation inhibitor might be a promising lead compound.

4. Materials and methods

4.1. Chemistry part

All reagents and solvents used were of analytical grade and were purchased from Zhengzhou Research Biotechnology Co., Ltd. ^1H NMR and ^{13}C NMR spectra were recorded on a Bruker 400 and 100 MHz spectrometer with TMS as internal standard in $\text{DMSO-}d_6$. High-resolution mass spectra (HRMS) were recorded on a Waters Micromass QT of Micromass spectrometer by electrospray ionization (ESI).

General procedure for the synthesis of compounds V1 ~ V17: Compound **IV** was synthesized according to our previous reference [23]. 5-Methoxy-1H-indole (10 mmol) and sodium hydroxide (10 mmol) was added to the solution of crude product **IV** (10 mmol) in acetone (15 mL). After stirring at 60 °C for 6 h, the reaction mixture was concentrated to remove then treated with a solution of ethyl acetate (20 mL) and H_2O (20 mL). The organic layer was washed with aqueous NaHCO_3 , water, and brine, dried over anhydrous Na_2SO_4 , and then concentrated. The residue was purified by column chromatography with petroleum/ethyl acetate (10:1) as an eluent to afford the target compounds **V1 ~ V17**. The NMR analysis of all indole derivatives was showed in the

Supporting information.

N-benzyl-2-(5-methoxy-1H-indol-1-yl)-N-(3,4,5-trimethoxyphenyl)acetamide (V1)

White solid, m.p.: 114 ~ 115 °C, yield: 45%. ^1H NMR (400 MHz, $\text{DMSO-}d_6$) δ 7.34 – 7.29 (m, 2H), 7.26 (dd, J = 10.3, 7.3 Hz, 3H), 7.17 (d, J = 8.9 Hz, 1H), 7.13 (t, J = 3.3 Hz, 1H), 7.04 (d, J = 2.4 Hz, 1H), 6.76 (dd, J = 8.8, 2.4 Hz, 1H), 6.57 (s, 2H), 6.32 (d, J = 2.9 Hz, 1H), 4.85 (t, J = 8.7 Hz, 4H), 3.75 (s, 3H), 3.69 (d, J = 6.4 Hz, 6H), 3.66 (s, 3H). ^{13}C NMR (100 MHz, $\text{DMSO-}d_6$) δ 167.30, 153.48, 153.05, 137.33, 137.01, 136.13, 131.57, 130.07, 128.39, 128.28, 128.23, 127.18, 110.94, 110.39, 105.88, 102.04, 100.42, 59.97, 55.92, 55.31, 52.48, 48.06. HRMS (ESI) (m/z) [$\text{M} + \text{H}$] $^+$ calcd for $\text{C}_{27}\text{H}_{29}\text{N}_2\text{O}_5$, 461.2076; found, 461.2078.

N-(4-fluorobenzyl)-2-(5-methoxy-1H-indol-1-yl)-N-(3,4,5-trimethoxyphenyl)acetamide (V2)

White solid, m.p.: 107 ~ 108 °C, yield: 85%. ^1H NMR (400 MHz, $\text{DMSO-}d_6$) δ 7.27 (dd, J = 8.2, 5.8 Hz, 2H), 7.19 – 7.10 (m, 4H), 7.03 (d, J = 2.3 Hz, 1H), 6.75 (dd, J = 8.8, 2.4 Hz, 1H), 6.57 (s, 2H), 6.31 (d, J = 2.9 Hz, 1H), 4.84 (d, J = 8.8 Hz, 4H), 3.75 (s, 3H), 3.71 (s, 6H), 3.66 (s, 3H). ^{13}C NMR (100 MHz, $\text{DMSO-}d_6$) δ 167.31, 162.60, 160.18, 153.48, 153.10, 137.05, 136.00, 133.57, 133.54, 131.58, 130.45, 130.37, 130.06, 128.38, 115.08, 114.87, 110.94, 110.40, 105.90, 102.03, 100.41, 59.97, 55.96, 55.31, 51.72, 48.05. HRMS (ESI) (m/z) [$\text{M} + \text{H}$] $^+$ calcd for $\text{C}_{27}\text{H}_{28}\text{FN}_2\text{O}_5$, 479.1982; found, 479.1987.

N-(4-chlorobenzyl)-2-(5-methoxy-1H-indol-1-yl)-N-(3,4,5-trimethoxyphenyl)acetamide (V3)

White solid, m.p.: 113 ~ 114 °C, yield: 72%. ^1H NMR (400 MHz, $\text{DMSO-}d_6$) δ 7.37 (d, J = 8.4 Hz, 2H), 7.26 (d, J = 8.3 Hz, 2H), 7.16 (d, J = 8.9 Hz, 1H), 7.10 (d, J = 2.9 Hz, 1H), 7.02 (d, J = 2.3 Hz, 1H), 6.74

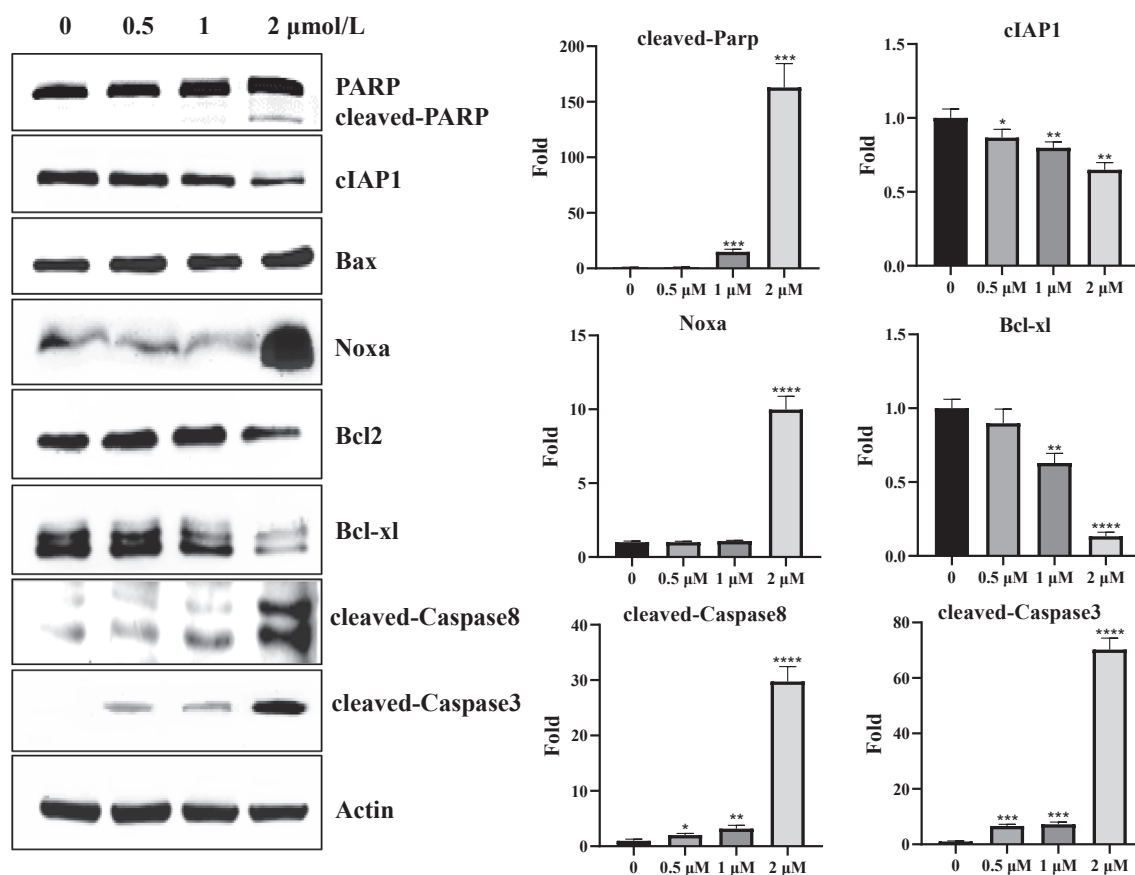


Fig. 6. The effects of V7 on apoptosis proteins, MGC803 cells were treated with V7 for 48 h. The results shown were representative of three independent experiments. *: $p < 0.05$ verse control. **: $p < 0.01$ verse control. ***: $p < 0.001$ verse control. ****: $p < 0.0001$ verse control.

(dd, $J = 8.8, 2.4$ Hz, 1H), 6.59 (s, 2H), 6.30 (d, $J = 2.9$ Hz, 1H), 4.84 (d, $J = 8.7$ Hz, 4H), 3.74 (s, 3H), 3.70 (d, $J = 13.2$ Hz, 6H), 3.65 (s, 3H). ^{13}C NMR (100 MHz, DMSO- d_6) δ 167.40, 153.47, 153.10, 137.04, 136.36, 136.03, 131.79, 131.57, 130.18, 130.07, 128.36, 128.20, 110.93, 110.41, 105.86, 102.03, 100.41, 59.98, 56.00, 55.32, 51.83, 48.030. HRMS (ESI) (m/z) [$M + H$] $^+$ calcd for $\text{C}_{27}\text{H}_{28}\text{ClN}_2\text{O}_5$, 495.1687; found, 495.1689.

***N*-(4-bromobenzyl)-2-(5-methoxy-1H-indol-1-yl)-*N*-(3,4,5-trimethoxyphenyl)acetamide (V4)**

White solid, m.p.:119 ~ 121 °C, yield: 77%. ^1H NMR (400 MHz, DMSO- d_6) δ 7.50 (d, $J = 8.3$ Hz, 2H), 7.19 (dd, $J = 15.3, 8.6$ Hz, 3H), 7.11 (d, $J = 2.9$ Hz, 1H), 7.03 (d, $J = 2.3$ Hz, 1H), 6.75 (dd, $J = 8.8, 2.4$ Hz, 1H), 6.60 (s, 2H), 6.31 (d, $J = 2.9$ Hz, 1H), 4.85 (d, $J = 8.6$ Hz, 2H), 4.82 (s, 2H), 3.75 (s, 3H), 3.72 (s, 6H), 3.66 (s, 3H). ^{13}C NMR (100 MHz, DMSO- d_6) δ 167.41, 153.49, 153.12, 137.07, 136.78, 136.04, 131.58, 131.12, 130.54, 130.06, 128.37, 120.32, 110.95, 110.41, 105.87, 102.04, 100.42, 59.98, 56.00, 55.32, 51.92, 48.04. HRMS (ESI) (m/z) [$M + H$] $^+$ calcd for $\text{C}_{27}\text{H}_{28}\text{BrN}_2\text{O}_5$, 539.1182; found, 539.1187.

***N*-(3-fluorobenzyl)-2-(5-methoxy-1H-indol-1-yl)-*N*-(3,4,5-trimethoxyphenyl)acetamide (V5)**

White solid, m.p.:114 ~ 115 °C, yield: 45%. ^1H NMR (400 MHz, DMSO- d_6) δ 7.38 – 7.31 (m, 1H), 7.18 (d, $J = 8.9$ Hz, 1H), 7.11 (dd, $J = 8.1, 4.2$ Hz, 2H), 7.08 (d, $J = 6.5$ Hz, 2H), 7.03 (d, $J = 2.3$ Hz, 1H), 6.75 (dd, $J = 8.8, 2.4$ Hz, 1H), 6.63 (s, 2H), 6.31 (d, $J = 2.9$ Hz, 1H), 4.87 (d, $J = 6.8$ Hz, 4H), 3.75 (s, 3H), 3.72 (s, 6H), 3.66 (s, 3H). ^{13}C NMR (100 MHz, DMSO- d_6) δ 167.52, 163.32, 160.90, 153.48, 153.11, 140.32, 140.25, 137.06, 136.08, 131.58, 130.21, 130.13, 130.08, 128.38, 124.24, 114.94, 114.73, 114.06, 113.85, 110.93, 110.43, 105.85, 102.03, 100.42, 59.97, 55.99, 55.31, 52.03, 48.05. HRMS (ESI) (m/z) [$M + H$] $^+$ calcd for $\text{C}_{27}\text{H}_{28}\text{FN}_2\text{O}_5$, 479.1982; found, 479.1989.

***2*-(5-Methoxy-1H-indol-1-yl)-*N*-(4-methylbenzyl)-*N*-(3,4,5-**

trimethoxyphenyl)acetamide (V6)

White solid, m.p.:96 ~ 97 °C, yield: 62%. ^1H NMR (400 MHz, DMSO- d_6) δ 7.15 (d, $J = 8.9$ Hz, 1H), 7.11 (s, 5H), 7.03 (d, $J = 2.4$ Hz, 1H), 6.75 (dd, $J = 8.8, 2.4$ Hz, 1H), 6.56 (s, 2H), 6.30 (d, $J = 2.9$ Hz, 1H), 4.84 (s, 2H), 4.79 (s, 2H), 3.75 (s, 3H), 3.69 (d, $J = 8.9$ Hz, 6H), 3.65 (s, 3H), 2.27 (s, 3H). ^{13}C NMR (100 MHz, DMSO- d_6) δ 167.19, 153.46, 153.02, 136.97, 136.29, 136.16, 134.27, 131.56, 130.08, 128.76, 128.55, 128.37, 128.28, 110.92, 110.38, 105.92, 102.03, 100.38, 100.16, 59.98, 55.95, 55.32, 52.20, 48.04, 20.65. HRMS (ESI) (m/z) [$M + H$] $^+$ calcd for $\text{C}_{28}\text{H}_{31}\text{N}_2\text{O}_5$, 475.2233; found, 475.2237.

***2*-(5-Methoxy-1H-indol-1-yl)-*N*-(4-methoxybenzyl)-*N*-(3,4,5-trimethoxyphenyl)acetamide (V7)**

White solid, m.p.:103 ~ 104 °C, yield: 50%. ^1H NMR (400 MHz, DMSO- d_6) δ 7.17 – 7.09 (m, 4H), 7.03 (d, $J = 2.3$ Hz, 1H), 6.86 (d, $J = 8.5$ Hz, 2H), 6.74 (dt, $J = 11.9, 6.0$ Hz, 1H), 6.52 (s, 2H), 6.30 (d, $J = 3.0$ Hz, 1H), 4.80 (d, $J = 13.3$ Hz, 2H), 4.76 (s, 2H), 3.74 (s, 3H), 3.71 (d, $J = 8.6$ Hz, 9H), 3.65 (s, 3H). ^{13}C NMR (100 MHz, DMSO- d_6) δ 178.96, 168.05, 162.86, 156.28, 152.78, 149.30, 139.04, 136.65, 133.86, 129.86, 129.24, 128.61, 125.30, 124.70, 124.13, 120.40, 34.84, 30.79. HRMS (ESI) (m/z) [$M + H$] $^+$ calcd for $\text{C}_{28}\text{H}_{31}\text{N}_2\text{O}_6$, 491.2182; found, 491.2189.

***2*-(5-Methoxy-1H-indol-1-yl)-*N*-(3-methylbenzyl)-*N*-(3,4,5-trimethoxyphenyl)acetamide (V8)**

White solid, m.p.:115 ~ 116 °C, yield: 72%. ^1H NMR (400 MHz, DMSO- d_6) δ 7.21 – 7.14 (m, 2H), 7.05 (dt, $J = 12.0, 10.6$ Hz, 5H), 6.75 (dd, $J = 8.8, 2.2$ Hz, 1H), 6.56 (s, 2H), 6.30 (d, $J = 2.8$ Hz, 1H), 4.86 (s, 2H), 4.80 (s, 2H), 3.75 (s, 3H), 3.70 (s, 6H), 3.65 (s, 3H), 2.27 (s, 3H). ^{13}C NMR (100 MHz, DMSO- d_6) δ 167.25, 153.49, 153.02, 137.32, 137.25, 137.02, 136.20, 131.54, 130.09, 128.83, 128.40, 128.11, 127.77, 125.35, 110.93, 110.36, 105.91, 102.08, 100.38, 59.98, 55.94, 55.34, 52.42, 48.12, 20.90. HRMS (ESI) (m/z) [$M + H$] $^+$ calcd for

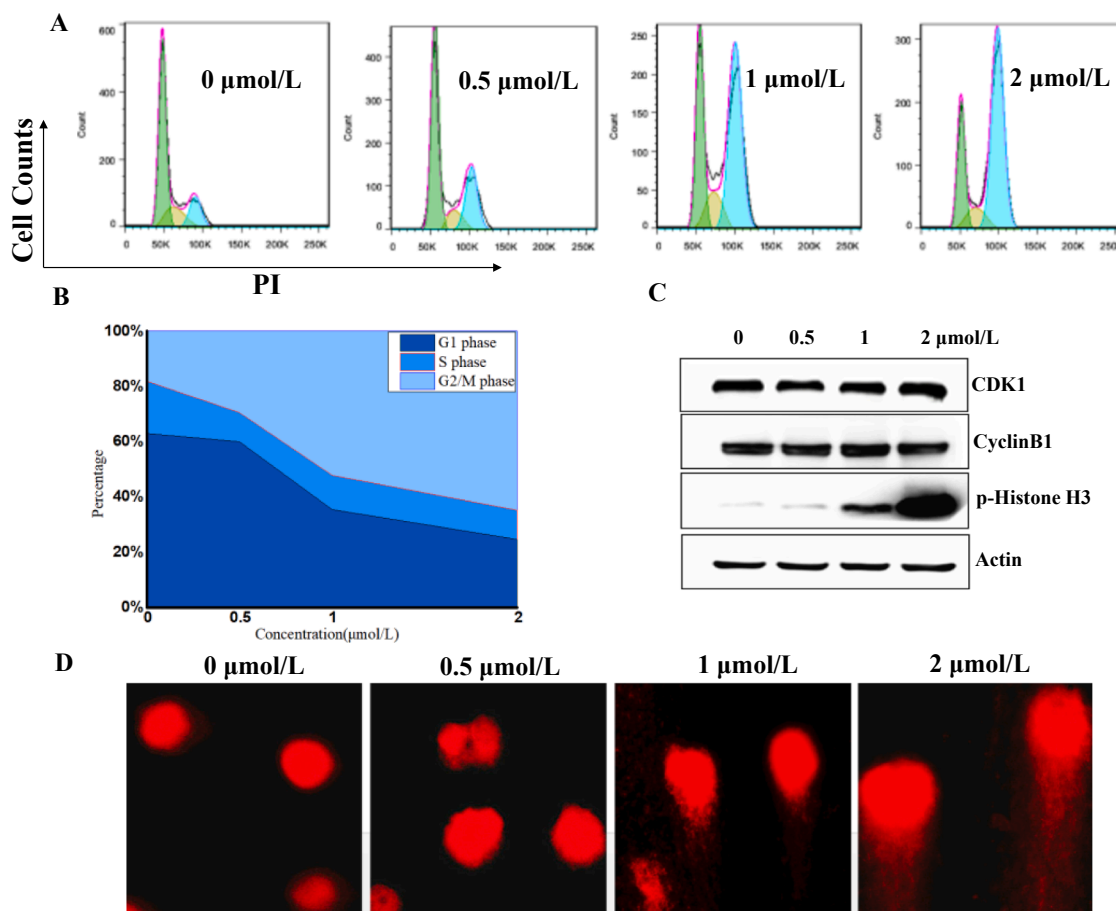


Fig. 7. A&B. MGC803 cells were stained by PI and cell cycle percentages were analyzed after 48 h treatment; C. The expression levels of CDK1, CyclinB1 and p-Histone H3 in MGC803 cells affected by V7; D. The comet assay.

$C_{28}H_{31}N_2O_5$, 475.2233; found, 475.2236.

***N*-(4-(*tert*-butyl)benzyl)-2-(5-methoxy-1*H*-indol-1-yl)-*N*-(3,4,5-trimethoxyphenyl)acetamide (V9)**

White solid, m.p.:46 ~ 47 °C, yield:45%. 1H NMR (400 MHz, DMSO- d_6) δ 7.37–7.28 (m, 2H), 7.25–7.05 (m, 4H), 7.04 (d, J = 2.2 Hz, 1H), 6.75 (dt, J = 9.4, 4.7 Hz, 1H), 6.43 (d, J = 68.3 Hz, 2H), 6.32 (t, J = 6.8 Hz, 1H), 4.83 (d, J = 12.2 Hz, 2H), 4.80 (s, 2H), 3.75 (s, 3H), 3.74–3.67 (m, 6H), 3.66 (s, 3H), 1.26 (s, 9H). ^{13}C NMR (100 MHz, DMSO- d_6) δ 167.13, 153.49, 153.22, 153.01, 149.63, 137.04, 136.09, 134.41, 131.59, 131.00, 130.07, 128.39, 128.19, 127.97, 125.65, 124.92, 111.90, 111.07, 110.93, 110.40, 106.01, 102.06, 101.64, 100.77, 100.39, 59.98, 55.87, 55.33, 55.22, 52.15, 48.06, 34.14, 31.08. HRMS (ESI) (m/z) [$M + H$] $^+$ calcd for $C_{31}H_{37}N_2O_5$, 517.2702; found, 517.2705.

***2*-(5-Methoxy-1*H*-indol-1-yl)-*N*-(2-methylbenzyl)-*N*-(3,4,5-trimethoxyphenyl)acetamide (V10)**

White solid, m.p.:108 ~ 110 °C, yield:70%. 1H NMR (400 MHz, DMSO- d_6) δ 7.19–7.10 (m, 6H), 7.03 (d, J = 2.3 Hz, 1H), 6.75 (dd, J = 8.8, 2.3 Hz, 1H), 6.55 (s, 2H), 6.31 (d, J = 2.9 Hz, 1H), 4.86 (d, J = 6.0 Hz, 4H), 3.75 (s, 3H), 3.68 (s, 6H), 3.64 (s, 3H), 2.15 (s, 3H). ^{13}C NMR (100 MHz, DMSO- d_6) δ 166.99, 153.47, 152.97, 137.05, 136.19, 135.74, 134.95, 131.58, 130.09, 129.91, 129.15, 128.38, 127.21, 125.63, 110.92, 110.38, 106.08, 102.06, 100.39, 60.01, 55.96, 55.34, 49.93, 48.06, 18.66. HRMS (ESI) (m/z) [$M + H$] $^+$ calcd for $C_{28}H_{31}N_2O_5$, 475.2233; found, 475.2238.

***N*-(3-chlorobenzyl)-2-(5-methoxy-1*H*-indol-1-yl)-*N*-(3,4,5-trimethoxyphenyl)acetamide (V11)**

White solid, m.p.:109 ~ 110 °C, yield: 80%. 1H NMR (400 MHz, DMSO- d_6) δ 7.47–7.21 (m, 2H), 7.18 (dd, J = 8.8, 5.6 Hz, 1H), 7.14–

7.07 (m, 3H), 7.04 (d, J = 2.3 Hz, 1H), 6.75 (dd, J = 8.8, 2.4 Hz, 1H), 6.62 (d, J = 9.0 Hz, 2H), 6.31 (d, J = 2.5 Hz, 1H), 4.93–4.80 (m, 4H), 3.75 (s, 3H), 3.72 (s, 6H), 3.66 (s, 3H). ^{13}C NMR (100 MHz, DMSO- d_6) δ 167.52, 163.32, 160.90, 153.48, 153.10, 140.31, 140.24, 139.85, 137.07, 136.08, 136.00, 132.88, 131.58, 131.55, 130.21, 130.12, 130.08, 128.38, 128.10, 127.17, 126.96, 124.24, 114.94, 114.72, 114.06, 113.85, 110.93, 110.42, 105.85, 102.04, 100.42, 59.98, 55.99, 55.32, 52.02, 51.93, 48.04. HRMS (ESI) (m/z) [$M + H$] $^+$ calcd for $C_{27}H_{28}ClN_2O_5$, 495.1687; found, 495.1689.

***2*-(5-Methoxy-1*H*-indol-1-yl)-*N*-(3-methoxybenzyl)-*N*-(3,4,5-trimethoxyphenyl)acetamide (V12)**

White solid, m.p.:97 ~ 98 °C, yield: 47% 1H NMR (400 MHz, DMSO- d_6) δ 7.23 (d, J = 6.5 Hz, 1H), 7.15 (dd, J = 14.5, 9.0 Hz, 2H), 7.04 (s, 1H), 6.78 (dd, J = 16.6, 11.2 Hz, 4H), 6.59 (d, J = 5.0 Hz, 2H), 6.31 (s, 1H), 4.85 (d, J = 11.9 Hz, 2H), 4.82 (s, 2H), 3.82–3.72 (m, 3H), 3.68 (dd, J = 19.0, 3.8 Hz, 12H). ^{13}C NMR (100 MHz, DMSO- d_6) δ 167.30, 159.20, 153.48, 153.04, 138.92, 137.05, 136.19, 131.57, 130.07, 129.29, 128.39, 120.45, 113.75, 112.68, 110.92, 110.38, 105.92, 102.06, 100.40, 59.98, 55.96, 55.33, 54.93, 52.42, 48.07. HRMS (ESI) (m/z) [$M + H$] $^+$ calcd for $C_{28}H_{31}N_2O_6$, 491.2182; found, 491.2187.

***N*-(3-(chloromethyl)benzyl)-2-(5-methoxy-1*H*-indol-1-yl)-*N*-(3,4,5-trimethoxyphenyl)acetamide (V13)**

White solid, m.p.:71 ~ 72 °C, yield: 64%. 1H NMR (400 MHz, DMSO- d_6) δ 7.33 (d, J = 4.3 Hz, 2H), 7.30 (s, 1H), 7.21 (s, 1H), 7.16 (d, J = 8.8 Hz, 1H), 7.12 (d, J = 2.5 Hz, 1H), 7.04 (d, J = 2.1 Hz, 1H), 6.76 (dd, J = 8.8, 2.2 Hz, 1H), 6.57 (s, 2H), 6.31 (d, J = 2.7 Hz, 1H), 4.87 (s, 4H), 4.73 (s, 2H), 3.75 (s, 3H), 3.70 (s, 6H), 3.65 (s, 3H). ^{13}C NMR (100 MHz, DMSO- d_6) δ 167.36, 153.50, 153.08, 137.82, 137.70, 137.04,

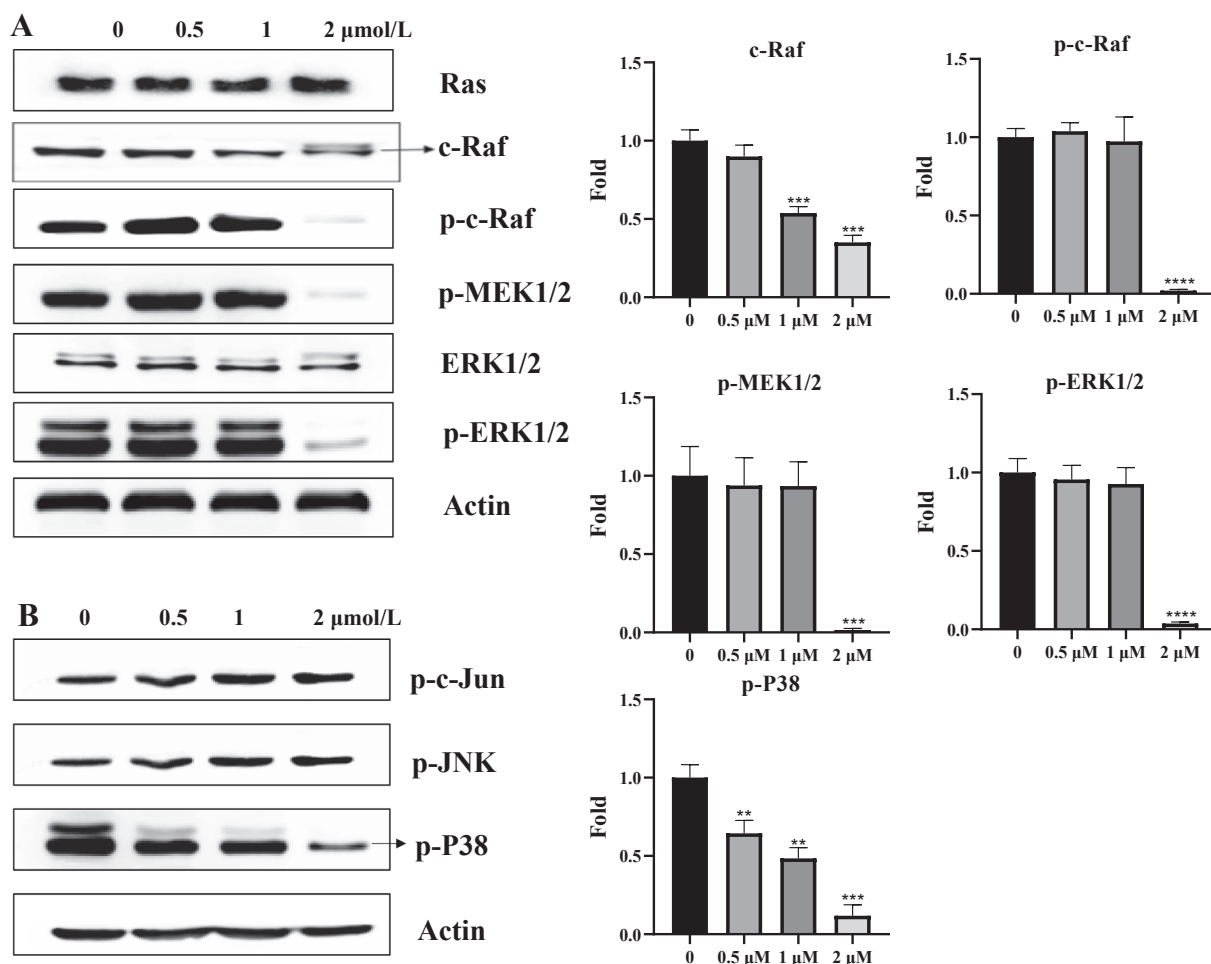


Fig. 8. A&B: The expression levels of V7 on MAPK pathway proteins, MGC803 cells were treated with V7 for 48 h. The results shown were representative of three independent experiments. **: $p < 0.01$ verse control. ***: $p < 0.001$ verse control. ****: $p < 0.0001$ verse control.

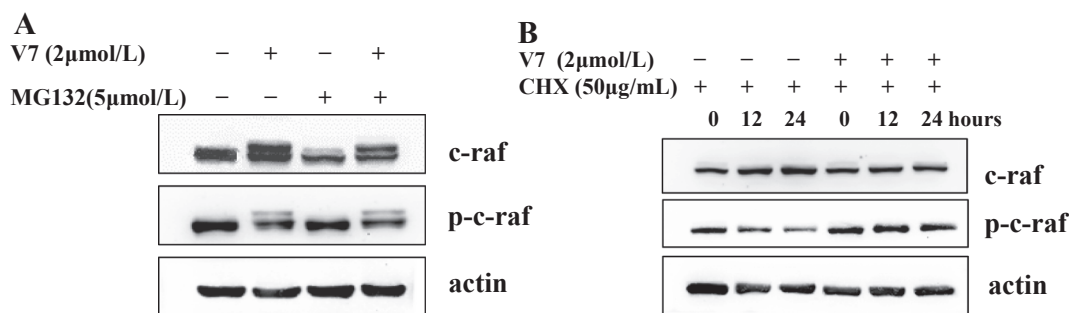


Fig. 9. A: MGC803 cells were treated by V7 with/without MG132 (a proteasome inhibitor) for 24 h; **B:** MGC803 cells were treated by V7 with/without CHX (cycloheximide) for different time.

136.07, 131.54, 130.08, 128.63, 128.54, 128.41, 128.32, 127.70, 110.94, 110.36, 105.84, 102.09, 100.41, 59.96, 55.93, 55.34, 52.23, 48.11, 46.06. HRMS (ESI) (m/z) [$M + H$]⁺ calcd for C₂₈H₃₀ClN₂O₅, 509.1843; found, 509.1847.

***N*-(3,5-dimethoxybenzyl)-2-(5-methoxy-1H-indol-1-yl)-*N*-(3,4,5-trimethoxyphenyl)acetamide (V14)**

Yellow solid, m.p.:46–47 °C, yield:50%. ¹H NMR (400 MHz, DMSO-*d*₆) δ 7.15 (d, $J = 8.9$ Hz, 1H), 7.11 (d, $J = 2.8$ Hz, 1H), 7.03 (d, $J = 2.3$ Hz, 1H), 6.74 (dd, $J = 8.8, 2.4$ Hz, 1H), 6.61 (s, 2H), 6.39 (s, 3H), 6.31 (d, $J = 2.9$ Hz, 1H), 4.88 (s, 2H), 4.78 (s, 2H), 3.75 (s, 3H), 3.72 (s, 6H), 3.68 (d, $J = 6.4$ Hz, 6H), 3.66 (s, 3H). ¹³C NMR (100 MHz, DMSO-*d*₆) δ 167.34, 160.36, 153.49, 153.04, 139.71, 137.07, 136.24,

131.56, 130.06, 128.40, 110.91, 110.36, 106.11, 105.91, 102.07, 100.40, 98.98, 59.98, 59.72, 55.97, 55.33, 55.08, 52.50, 48.10. HRMS (ESI) (m/z) [$M + H$]⁺ calcd for C₂₉H₃₃N₂O₇, 521.2288; found, 521.2289.

2-(5-Methoxy-1H-indol-1-yl)-*N*-(4-methoxybenzyl)-*N*-phenylacetamide (V15)

Yellow solid, m.p.:44 ~ 45 °C, yield:55% ¹H NMR (400 MHz, DMSO) δ 7.46 (t, $J = 7.2$ Hz, 2H), 7.39 (d, $J = 6.7$ Hz, 1H), 7.33 (d, $J = 7.4$ Hz, 2H), 7.16 (d, $J = 2.5$ Hz, 1H), 7.11 (t, $J = 7.4$ Hz, 3H), 7.04 (d, $J = 2.3$ Hz, 1H), 6.84 (d, $J = 8.4$ Hz, 2H), 6.76 (dd, $J = 8.8, 2.4$ Hz, 1H), 6.32 (d, $J = 2.9$ Hz, 1H), 4.80 (d, $J = 13.9$ Hz, 2H), 4.72 (s, 2H), 3.75 (s, 3H), 3.72 (s, 3H). ¹³C NMR (100 MHz, DMSO) δ 166.91, 158.41, 153.49, 140.68,

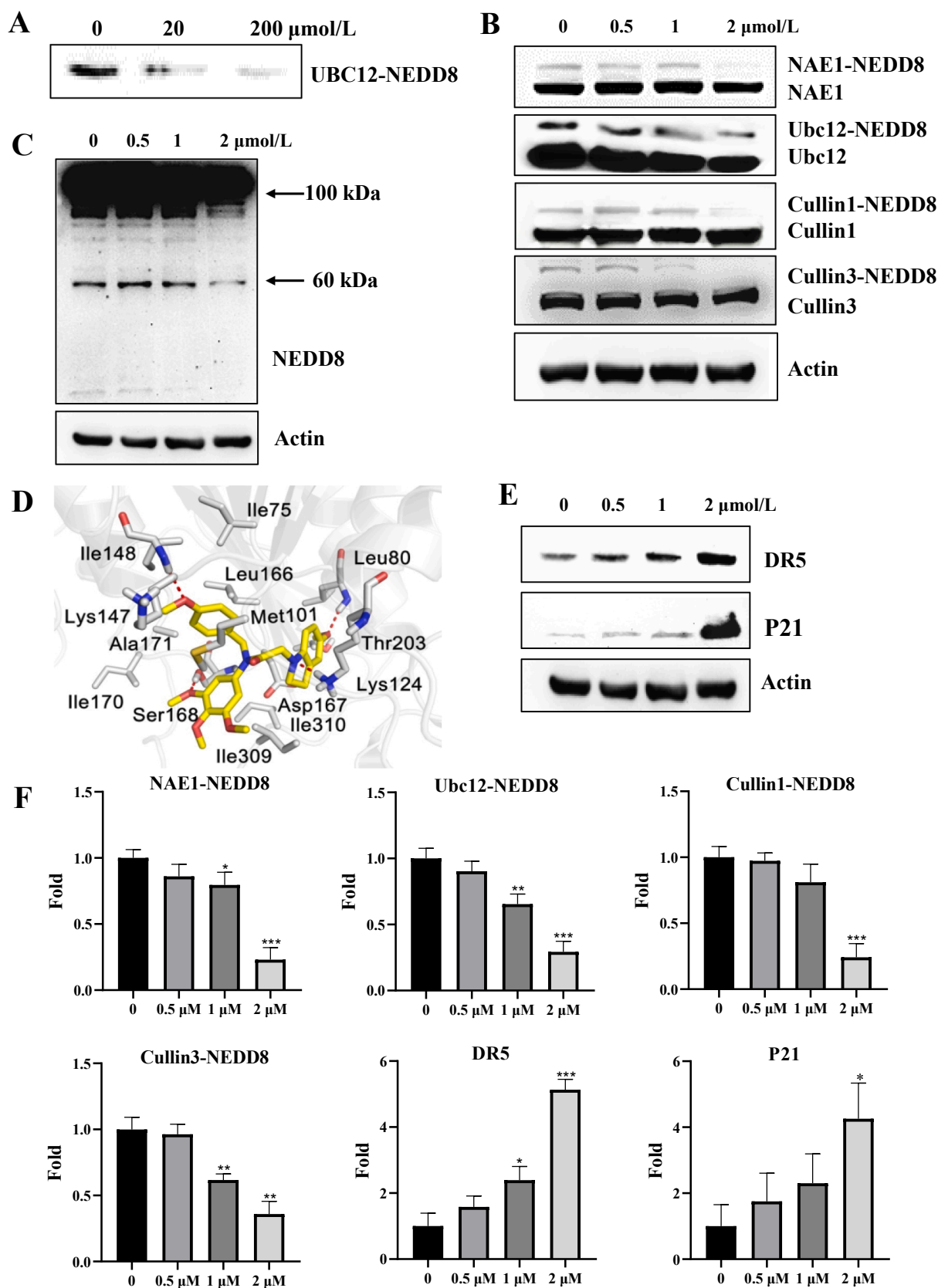


Fig. 10. A. An *in vitro* NEDD8 conjugation assay out of cells; B&C. The effect of V7 on NEDDylation, MGC803 cells were treated with V7 for 48 h; D. Docking results of compound V7 that interacted with NAE (PDB code: 3GZN); E. The expression levels of NEDDylation substrates (DR5 and P21) by compound V7; F. Statistical analysis of proteins expression in MGC803 cells. The results shown were representative of three independent experiments. *: $p < 0.05$ verse control. **: $p < 0.01$ verse control. ***: $p < 0.001$ verse control.

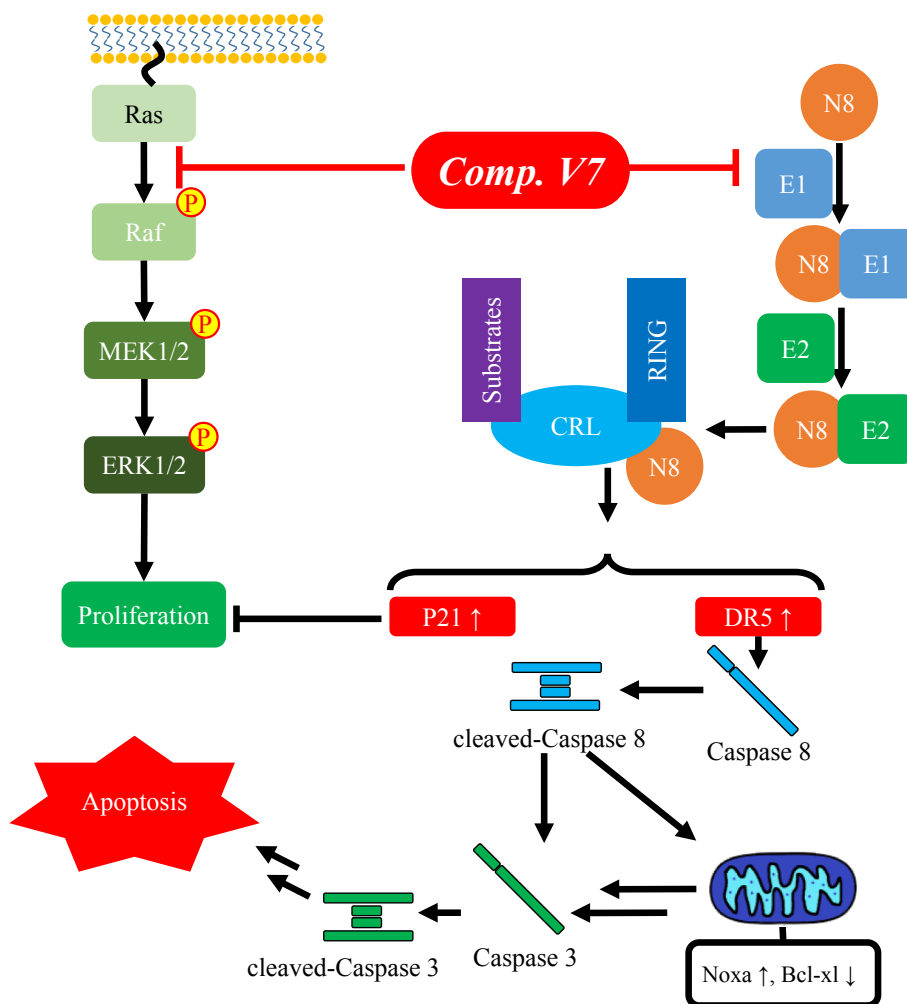


Fig. 11. V7 inhibits NEDDylation and MAPK pathways against gastric cancer MGC803 cells.

131.59, 130.32, 129.68, 129.47, 129.01, 128.45, 128.31, 113.67, 111.00, 110.22, 102.14, 100.35, 55.33, 54.96, 51.88, 47.85. HRMS (ESI) (m/z) [$M + H$]⁺ calcd for $C_{25}H_{25}N_2O_3$, 401.1865; found, 401.1869.

2-(5-Methoxy-1H-indol-1-yl)-N-(4-methoxybenzyl)-N-(4-methoxyphenyl)acetamide (V16)

Yellow solid, m.p.:48 ~ 49 °C, yield:75%. ¹H NMR (400 MHz, DMSO-*d*₆) δ 7.23 (d, *J* = 8.8 Hz, 2H), 7.16 (d, *J* = 3.0 Hz, 1H), 7.10 (dd, *J* = 8.4, 6.4 Hz, 3H), 7.04 (d, *J* = 2.3 Hz, 1H), 6.99 (t, *J* = 7.7 Hz, 2H), 6.85 (d, *J* = 8.6 Hz, 2H), 6.76 (dd, *J* = 8.8, 2.4 Hz, 1H), 6.32 (d, *J* = 2.9 Hz, 1H), 4.76 (s, 2H), 4.65 (d, *J* = 35.1 Hz, 2H), 3.76 (d, *J* = 4.5 Hz, 6H), 3.74 – 3.71 (m, 3H). ¹³C NMR (100 MHz, DMSO-*d*₆) δ 167.16, 158.70, 158.40, 153.47, 133.18, 131.60, 130.33, 129.55, 129.50, 129.12, 128.87, 128.44, 128.29, 128.17, 114.78, 114.55, 113.65, 110.97, 110.21, 102.12, 100.31, 55.33, 55.28, 54.95, 51.96, 47.75. HRMS (ESI) (m/z) [$M + H$]⁺ calcd for $C_{26}H_{27}N_2O_4$, 431.1971; found, 431.1975.

N-(3,4-dimethoxyphenyl)-2-(5-methoxy-1H-indol-1-yl)-N-(4-methoxybenzyl)acetamide (V17)

White solid, m.p.:49 ~ 50 °C, yield:55%. ¹H NMR (400 MHz, DMSO-*d*₆) δ 7.12 (dd, *J* = 15.0, 5.4 Hz, 4H), 7.04 (d, *J* = 2.3 Hz, 1H), 6.96 (d, *J* = 8.5 Hz, 1H), 6.86 (s, 2H), 6.84 (s, 1H), 6.81 – 6.72 (m, 2H), 6.31 (d, *J* = 2.9 Hz, 1H), 4.75 (d, *J* = 7.8 Hz, 4H), 3.76 (d, *J* = 3.4 Hz, 6H), 3.72 (d, *J* = 3.5 Hz, 6H). ¹³C NMR (101 MHz, DMSO-*d*₆) δ 167.17, 158.43, 153.47, 149.08, 148.42, 133.22, 131.60, 130.27, 129.69, 129.26, 128.42, 120.47, 113.62, 112.03, 111.73, 110.93, 110.28, 102.11, 100.29, 55.58, 55.52, 55.34, 54.98, 51.87, 47.81. HRMS (ESI) (m/z) [$M + H$]⁺ calcd for $C_{27}H_{29}N_2O_5$, 461.2076; found, 461.2079.

4.2. Cell culture and MTT assay

Cell lines were cultured at 37 °C in an atmosphere containing 5% CO₂, RPMI-1640 medium with 10% fetal bovine serum, 100 U/ml penicillin and 0.1 mg/ml streptomycin was used as culture medium (Servicebio, Wuhan, China). Cells were seeded at a density of 5×10^3 per well in 96-well plates for 24 h and treated with compound for 48 h. Then, 20 μL MTT solution (Servicebio, Wuhan, China) was added to each well, and incubated for 4 h at 37 °C. 150 μL DMSO was added to each well to dissolve the formazan after removing the supernatant liquid, the absorbance was determined at 570 nm.

4.3. Colony formatting assay

MGC803 cells were seeded in a 6-well plate and incubated in 5% CO₂ at 37 °C for 24 h, then treated with different concentration of compound. After 7 days, remove the culture medium, wash the cells twice with PBS, fix cells with 4% paraformaldehyde and stain with 0.1% crystal violet. The cells' images were captured with microscope (Nikon, Japan).

4.4. Cell cycle distribution assay

MGC803 cells were seeded in 6-well culture plate and treated with compound for 48 h. Then cells were harvested and fixed with 70% ethanol for 8 h at 4 °C. The fixed cells were washed and resuspended with PBS containing 50 mg/mL and PI 10 mg/mL RNaseA (Servicebio, Wuhan, China). Then cell suspension was incubated for 30 min in a dark

place. After that, samples were analyzed for DNA content with flow cytometry. (Becton, Dickinson and Company, NJ).

4.5. Cell apoptosis assay

MGC803 cells were seeded in 6-well culture plate and treated with compound for 48 h. Then cells were harvested and resuspended in binding buffer containing Annexin V-FITC (0.5 mg/mL) and PI (0.5 mg/mL) and incubated for 30 min in a dark place. After that, samples were analyzed with flow cytometry (Becton, Dickinson and Company, NJ).

4.6. Comet assay

MGC803 cells were treated with different concentration of compound for 48 h. Then the cells were harvested and covered with comet slides. The slides were immersed in the lysis buffer at 4 °C for 2 h. After lysed, Comet slides were immersed in cold electrophoresis buffer for 25 min to equilibrate the slides. Then, electrophoresis was conducted at 25 V, 300 mA, for 30 min. Then the slides coated with drops of neutralization buffer for 5 min. The slides were stained with 1.0 µg/ml DAPI, and observed with a fluorescent microscope (Nikon, Japan).

4.7. Western blotting analysis

MGC803 cells were treated with different concentration of compound harvested and lysed. Protein lysates were denatured and resolved by SDS-PAGE and transferred to nitrocellulose membrane. The membranes were incubated with appropriate antibodies for 8 h at 4 °C after blocking with 5% skimmed milk. After conjugated with secondary antibodies, the detection of proteins was carried out with an ECL kit.

4.8. In vitro NEDD8 conjugation assay

The *in vitro* NEDD8 conjugation assay kit was purchased from abcam (Cambridge, MA). A master mix of APPBP1/Uba3, UbcH12 and NEDD8 were prepared in the reaction buffer and distributed to individual tubes. Different concentration of compound was added to the indicated tubes and mixed well. The reactions were started by adding 2.5 mM Mg²⁺ + and 1 mM ATP. The reaction tubes were incubated in 37 °C for 30 min. Western blot was performed with anti-NEDD8 antibody to detect Nedd8 conjugated Ubc12 bands.

4.9. Docking study

All the molecular docking studies were performed using Autodock 4.2.6 software package. The crystal structure of NAE (PDB code: 3GZN) was retrieved from the RCSB Protein Data Bank. This structure was prepared by adding missing side chain atoms and hydrogen atoms, removing waters and taking structural optimization in Amber10: EHT force field. The three-dimensional structure of compound V7 was built in MOE, and were taken energy minimization and conformational search before docking. The protonation states of both receptor proteins and compound V7 were determined at pH = 7. Then the ligand was docked into the binding sites of NAE with default parameters in Amber10: EHT force field, and 20 docking poses were exported for further visual analysis.

4.10. Statistical analysis

Data from three independent experiments are presented as mean ± SD. IC₅₀ values and SD values were calculated by SPSS version 10.0 (SPSS, Inc., Chicago, IL, USA).

Declaration of Competing Interest

The authors declared that there is no conflict of interest.

Acknowledgment

This research was funded by the National Natural Sciences Foundations of China (No. 81703541 & U2004123 for Sai-Yang Zhang and No. 81673322 for Yan-Bing Zhang), China Postdoctoral Science Foundation (No. 2018M632812 for Sai-Yang Zhang), Henan Association of Science and Technology (No. 2020HYTP056 for Sai-Yang Zhang, China), Science and Technology Department of Henan Province (No. 20202310144, for Sai-Yang Zhang, China), the open fund of state key laboratory of Pharmaceutical Biotechnology, Nan-jing University, China (Grant no. KF-GN-202104). The manuscript was also supported by China Postdoctoral Science Foundation (Grant no. 2020M670239).

Appendix A. Supplementary data

Supplementary data to this article can be found online at <https://doi.org/10.1016/j.bioorg.2021.104634>.

References

- [1] M. Yang, Y. Jin, S. Fan, X. Liang, J. Jia, Z. Tan, T. Huang, Y. Li, T. Ma, M. Li, Inhibition of neddylation causes meiotic arrest in mouse oocyte, *Cell Cycle* 18 (2019) 1–14.
- [2] S. Zhou, X. Zhao, Z. Yang, R. Yang, C. Chen, K. Zhao, W. Wang, Y. Ma, Q. Zhang, X. Wang, Neddylation inhibition upregulates PD-L1 expression and enhances the efficacy of immune checkpoint blockade in glioblastoma, *Int. J. Cancer* 145 (2019) 763–774.
- [3] A.K. Jayabalan, A. Sanchez, R.Y. Park, S.P. Yoon, G.-Y. Kang, J.-H. Baek, P. Anderson, Y. Kee, T. Ohn, Neddylation promotes stress granule assembly, *Nat. Commun.* 7 (2016) 12125.
- [4] Q. Zhang, D. Hou, Z. Luo, P. Chen, B. Lv, L. Wu, Y. Ma, Y. Chu, H. Liu, F. Liu, S. Yu, J. Zhang, D. Yang, J. Liu, The novel protective role of P27 in MLN4924-treated gastric cancer cells, *Cell Death Dis.* 6 (2015), e1867.
- [5] H. Lan, Z. Tang, H. Jin, Y. Sun, Neddylation inhibitor MLN4924 suppresses growth and migration of human gastric cancer cells, *Sci. Rep.* 6 (2016) 24218.
- [6] H. Li, M. Tan, L. Jia, D. Wei, Y. Zhao, G. Chen, J. Xu, L. Zhao, D. Thomas, D.G. Beer, Y. Sun, Inactivation of SAG/RBX2 E3 ubiquitin ligase suppresses KrasG12D-driven lung tumorigenesis, *J. Clin. Investig.* 124 (2014) 835–846.
- [7] T.-J. Ai, J.-Y. Sun, L.-J. Du, C. Shi, C. Li, X.-N. Sun, Y. Liu, L. Li, Z. Xia, L. Jia, J. Liu, S.-Z. Duan, Inhibition of neddylation by MLN4924 improves neointimal hyperplasia and promotes apoptosis of vascular smooth muscle cells through p53 and p62, *Cell Death Differ.* 25 (2018) 319–329.
- [8] C. Yoshimura, H. Muraoka, H. Ochiwa, S. Tsuji, A. Hashimoto, H. Kazuno, F. Nakagawa, Y. Komiya, S. Suzuki, T. Takenaka, M. Kumazaki, N. Fujita, T. Mizutani, S. Ohkubo, TAS4464, a highly potent and selective inhibitor of NEDD8 activating enzyme, suppresses neddylation and shows antitumor activity in diverse cancer models, *Mol. Cancer Ther.* 18 (2019) 1205–1216.
- [9] L. Zhou, Y. Jiang, Q. Luo, L. Li, L. Jia, Neddylation: a novel modulator of the tumor microenvironment, *Mol. Cancer.* 18 (2019) 77.
- [10] X. Jia, C. Li, L. Li, X. Liu, L. Zhou, W. Zhang, S. Ni, Y. Lu, L. Chen, L.S. Jeong, J. Yu, Y. Zhang, J. Zhang, S. He, X. Hu, H. Sun, K. Yu, G. Liu, H. Zhao, Y. Zhang, L. Jia, Z.-M. Shao, Neddylation Inactivation Facilitates FOXO3a Nuclear Export to Suppress Estrogen Receptor Transcription and Improve Fulvestrant Sensitivity, *Clin. Cancer Res.* 25 (2019) 3658–3672.
- [11] B. Xu, Y. Deng, R. Bi, H. Guo, C. Shu, N.K. Shah, J. Chang, G. Liu, Y. Du, W. Wei, C. Wang, A first-in-class inhibitor, MLN4924 (pevonedistat), induces cell-cycle arrest, senescence, and apoptosis in human renal cell carcinoma by suppressing UBE2M-dependent neddylation modification, *Cancer Chemoth. Pharm.* 81 (2018) 1083–1093.
- [12] J.T. Hammill, D.C. Scott, J. Min, M.C. Connelly, G. Holbrook, F. Zhu, A. Matheny, L. Yang, B. Singh, B.A. Schulman, R.K. Guy, Piperidiny Ureas Chemically Control Defective in Cullin Neddylation 1 (DCN1)-Mediated Cullin Neddylation, *J. Med. Chem.* 61 (2018) 2680–2693.
- [13] P. Lu, Y. Guo, L. Zhu, Y. Xia, Y. Zhong, Y. Wang, A novel NAE/UAE dual inhibitor LP0040 blocks neddylation and ubiquitination leading to growth inhibition and apoptosis of cancer cells, *Eur. J. Med. Chem.* 154 (2018) 294–304.
- [14] H. An, A.V. Statsyuk, An inhibitor of ubiquitin conjugation and aggregates formation, *Chem. Sci.* 6 (2015) 5235–5245.
- [15] W. Zhou, L. Ma, L. Ding, Q. Guo, Z. He, J. Yang, H. Qiao, L. Li, J. Yang, S. Yu, L. Zhao, S. Wang, H.-M. Liu, Z. Suo, W. Zhao, Potent 5-Cyano-6-phenyl-pyrimidin-Based Derivatives Targeting DCN1–UBE2M Interaction, *J. Med. Chem.* 62 (2019) 5382–5403.
- [16] S. Wang, L. Zhao, X.-J. Shi, L. Ding, L. Yang, Z.-Z. Wang, D. Shen, K. Tang, X.-J. Li, M.A.A. Mamun, H. Li, B. Yu, Y.-C. Zheng, S. Wang, H.-M. Liu, Development of Highly Potent, Selective, and Cellular Active Triazolo[1,5-a]pyrimidine-Based Inhibitors Targeting the DCN1–UBC12 Protein-Protein Interaction, *J. Med. Chem.* 62 (2019) 2772–2797.
- [17] X. Li, V. Pham, M. Tippin, D. Fu, R. Rendon, L. Song, E. Uchio, B.H. Hoang, X. Zi, Flavokawain B targets protein neddylation for enhancing the anti-prostate cancer effect of Bortezomib via Skp2 degradation, *Cell. Commun. Signal.* 17 (2019) 25.

- [18] S. Dadashpour, S. Emami, Indole in the target-based design of anticancer agents: A versatile scaffold with diverse mechanisms, *Eur. J. Med. Chem.* 150 (2018) 9–29.
- [19] N. Chadha, O. Silakari, Indoles as therapeutics of interest in medicinal chemistry: Bird's eye view, *Eur. J. Med. Chem.* 134 (2017) 159–184.
- [20] M.-Z. Zhang, Q. Chen, G.-F. Yang, A review on recent developments of indole-containing antiviral agents, *Eur. J. Med. Chem.* 89 (2015) 421–441.
- [21] J. Xu, H. He, L.-J. Zhou, Y.-Z. Liu, D.-W. Li, F.-L. Jiang, Y. Liu, Pyridinium and indole orientation determines the mitochondrial uncoupling and anti-cancer efficiency of F16, *Eur. J. Med. Chem.* 154 (2018) 305–313.
- [22] E.S. Shchegravina, A.A. Maleev, S.K. Ignatov, I.A. Gracheva, A. Stein, H.-G. Schmalz, A.E. Gavryushin, A.A. Zubareva, E.V. Svirshchevskaya, A.Y. Fedorov, Synthesis and biological evaluation of novel non-racemic indole-containing allocolchicinoids, *Eur. J. Med. Chem.* 141 (2017) 51–60.
- [23] D.J. Fu, S.Y. Zhang, Y.C. Liu, L. Zhang, J.J. Liu, J. Song, R.H. Zhao, F. Li, H.H. Sun, H.M. Liu, Design, synthesis and antiproliferative activity studies of novel dithiocarbamate-chalcone derivatives, *Bioorg. Med. Chem. Lett.* 26 (2016) 3918.
- [24] D.-J. Fu, J.-J. Yang, P. Li, Y.-H. Hou, S.-N. Huang, M.A. Tippin, V. Pham, L. Song, X. Zi, W.-L. Xue, L.-R. Zhang, S.-Y. Zhang, Bioactive heterocycles containing a 3,4,5-trimethoxyphenyl fragment exerting potent antiproliferative activity through microtubule destabilization, *Eur. J. Med. Chem.* 157 (2018) 50–61.
- [25] D.J. Fu, L. Zhang, J. Song, R.W. Mao, R.H. Zhao, Y.C. Liu, Y.H. Hou, J.H. Li, J. Yang, C.Y. Jin, Design and synthesis of formononetin-dithiocarbamate hybrids that inhibit growth and migration of PC-3 cells via MAPK/Wnt signaling pathways, *Eur. J. Med. Chem.* 127 (2016) 87–99.
- [26] D.J. Fu, J. Song, Y.H. Hou, R.H. Zhao, J.H. Li, R.W. Mao, J.J. Yang, P. Li, X.L. Zi, Z. H. Li, Discovery of 5,6-diaryl-1,2,4-triazines hybrids as potential apoptosis inducers, *Eur. J. Med. Chem.* 138 (2017) 1076–1088.
- [27] D.-J. Fu, S.-Y. Zhang, Y.-C. Liu, X.-X. Yue, J.-J. Liu, J. Song, R.-H. Zhao, F. Li, H.-H. Sun, Y.-B. Zhang, H.-M. Liu, Design, synthesis and antiproliferative activity studies of 1,2,3-triazole-chalcones, *MedChemComm.* 7 (2016) 1664–1671.
- [28] D.-J. Fu, R.-H. Zhao, J.-H. Li, J.-J. Yang, R.-W. Mao, B.-W. Wu, P. Li, X.-L. Zi, Q.-Q. Zhang, H.-J. Cai, S.-Y. Zhang, Y.-B. Zhang, H.-M. Liu, Molecular diversity of phenothiazines: design and synthesis of phenothiazine-dithiocarbamate hybrids as potential cell cycle blockers, *Mol. Divers.* 21 (2017) 933–942.
- [29] D.J. Fu, J.F. Liu, R.H. Zhao, J.H. Li, S.Y. Zhang, Y.B. Zhang, Design and Antiproliferative Evaluation of Novel Sulfanilamide Derivatives as Potential Tubulin Polymerization Inhibitors, *Molecules* 22 (2017) 1470.
- [30] S.-Y. Zhang, D.-J. Fu, X.-X. Yue, Y.-C. Liu, J. Song, H.-H. Sun, H.-M. Liu, Y.-B. Zhang, Design, Synthesis and Structure-Activity Relationships of Novel Chalcone-1,2,3-triazole-azole Derivates as Antiproliferative Agents, *Molecules* 21 (2016) 653.
- [31] D.J. Fu, L. Fu, Y.C. Liu, J.W. Wang, Y.Q. Wang, B.K. Han, X.R. Li, C. Zhang, F. Li, J. Song, Structure-Activity Relationship Studies of β -Lactam-azide Analogues as Orally Active Antitumor Agents Targeting the Tubulin Colchicine Site, *Sci. Rep.* 7 (2017) 12788.
- [32] D.-J. Fu, P. Li, J. Song, S.-Y. Zhang, H.-Z. Xie, Mechanisms of synergistic neurotoxicity induced by two high risk pesticide residues-Chlorpyrifos and Carbofuran via oxidative stress, *Toxicol. In Vitro* 54 (2019) 338–344.
- [33] S. Elmore, Apoptosis: a review of programmed cell death, *Toxicol. Pathol.* 35 (4) (2007) 495–516.
- [34] J.-S. Yang, R.-C. Lin, Y.-H. Hsieh, H.-H. Wu, G.-C. Li, Y.-C. Lin, S.-F. Yang, K.-H. Lu, CLEFMA Activates the Extrinsic and Intrinsic Apoptotic Processes through JNK1/2 and p38 Pathways in Human Osteosarcoma Cells, *Molecules* 24 (2019) 3280.
- [35] F. Baska, A. Sipos, Z. Örfi, Z. Nemes, J. Dobos, C. Szántai-Kis, E. Szabó, G. Szénási, L. Dézsi, P. Hamar, M.T. Cserepes, J. Tóvári, R. Garamvölgyi, M. Krekó, L. Örfi, Discovery and development of extreme selective inhibitors of the ITD and D835Y mutant FLT3 kinases, *Eur. J. Med. Chem.* 184 (2019), 111710.
- [36] G. Juan, T.L. Bush, C. Ma, R. Manoukian, G. Chung, J.M. Hawkins, S. Zoog, R. Kendall, R. Radinsky, R. Loberg, G. Friberg, M. Payton, AMG 900, a potent inhibitor of aurora kinases causes pharmacodynamic changes in p-Histone H3 immunoreactivity in human tumor xenografts and proliferating mouse tissues, *J. Transl. Med.* 12 (2014) 307.
- [37] Z. He, H. Qiao, F. Yang, W. Zhou, Y. Gong, X. Zhang, H. Wang, B. Zhao, L. Ma, H.-M. Liu, W. Zhao, Novel thiosemicarbazone derivatives containing indole fragment as potent and selective anticancer agent, *Eur. J. Med. Chem.* 184 (2019), 111764.
- [38] S. Al Bitar, H. Gali-Muhtasib, The Role of the Cyclin Dependent Kinase Inhibitor p21cip1/waf1 in Targeting Cancer: Molecular Mechanisms and Novel Therapeutics, *Cancers (Basel)* 11 (2019) 1475.
- [39] I. Shimizu, Y. Yoshida, M. Suda, T. Minamino, DNA Damage Response and Metabolic Disease, *Cell Metab.* 20 (2014) 967–977.
- [40] M. Burotto, V.L. Chiou, J.-M. Lee, E.C. Kohn, The MAPK pathway across different malignancies: a new perspective, *Cancer* 120 (2014) 3446–3456.
- [41] M.J. Robinson, M.H. Cobb, Mitogen-activated protein kinase pathways, *Curr. Opin. Cell Biol.* 9 (1997) 180–186.
- [42] T. Wada, J.M. Penninger, Mitogen-activated protein kinases in apoptosis regulation, *Oncogene* 23 (2004) 2838–2849.
- [43] S.-Y. Wang, X. Liu, Y. Liu, H.-Y. Zhang, Y.-B. Zhang, C. Liu, J. Song, J.-B. Niu, S.-Y. Zhang, Review of NEDDylation inhibition activity detection methods, *Bioorg. Med. Chem.* 29 (2021), 115875.